Inorganic Chemistry
Article

Inorg. Chem. **2010**, *49*, 3449–3460 **3449**
DOI: 10.1021/ic100002c

Synthesis and Characterization of *anti*-bisFe(III) Porphyrins, *syn*-bisFe(III)-μ-oxo Porphyrin, and *syn*-bisFe(III)-μ-oxo Porphyrin Cation Radical

Sudip Kumar Ghosh, Ranjan Patra, and Sankar Prasad Rath*

Department of Chemistry, Indian Institute of Technology Kanpur, Kanpur-208016, India

Received January 1, 2010

BisFe(III) porphyrins bridged by a highly flexible ethane linker are reported in which the bisporphyrin platform "opens" and "closes" its binding pockets leading to facile *syn-anti* conformational switching with very high vertical flexibility in a single molecular framework. With axial ligand X (X: Cl, Br, I, ClO_4), the *anti*-forms of the molecule are stabilized. The X-ray structure of *anti* bis perchloratoFe(III)porphyrin is reported, and the molecule is found to be high-spin in nature. In sharp contrast, all other Fe(III) porphyrins with ClO_4 as axial ligands are in an either intermediate or admixed spin state. The very strong Fe−$OClO_3$ bond and relatively weaker Fe−N(p) bonds are responsible for the high-spin nature of the molecule. Upon treatment with base, bis Fe(III)-μ-oxo porphyrin is generated in which the Fe−O−Fe unit is remarkably bent (with a 147.9(1)° angle) and two porphyrin rings in a molecule are so close that at least six carbon atoms from each of the porphyrin macrocycles are driven to be essentially closer than the van der Waals contact distance. Upon manipulating the acidity/basicity of the solution, the facile *syn-anti* conformational switching takes place that is also reversible in nature. The complex catalyzes the rapid photoinduced oxygenation of phosphites under mild condition using aerial O_2. Electrochemical data reveals that bis Fe(III)-μ-oxo porphyrin undergoes four one electron oxidations and one electron reduction. However, oxidations become easier in *syn* Fe(III)-μ-oxo dimer rather than the *anti*-form of the molecule (with axial ligand X). The presence of two porphyrin macrocycles within a short distance in the *syn* form makes the porphyrin core highly nonplanar and more electron rich, and that might be responsible for easier oxidations compared to $[Fe(OEP)]_2O$. Oxidations of the μ-oxo complex are performed using both chemical and electrochemical methods. The addition of 1.00 mol equiv of iodine−silver perchlorate generates the singly oxidized product that shows large isotropic shifts in ^1H NMR with eight diastereotopic methylene proton signals (at 295 K) spreading over 8 to 16 ppm, and two *meso* resonances occurs at −10.2 and −13.7 ppm in 2:1 ratio. However, the addition of less than 1 equiv of oxidizing agent gives an average ^1H NMR signal. This indicates that intra- and intermolecular electron transfer is rapid in the NMR time scale, and no porphyrin structural modification has occurred during oxidation.

Introduction

Porphyrin dimers have been attracting considerable attention as biomimetic models of photosynthetic systems, and as photonic materials and functional molecular devices.[1−8] Two porphyrins linked in a face-to-face arrangement by some rigid/flexible linkers form molecular clefts for the binding and activation of a variety of small molecules (e.g., O_2, N_2 and H_2). Since the type of bond connecting the porphyrin rings influences the electronic communication in the dimer, a variety of porphyrin arrays has been explored. In this regard, the reactivity of photoactive iron bisporphyrins is of recent interest,[2,3] owing to the ability of these systems to utilize molecular oxygen for substrate oxidations via the formation of bisiron(III) μ-oxo porphyrins. The bisporphyrins with significant vertical flexibility are particularly effective at

---

*To whom correspondence should be addressed. E-mail: sprath@iitk.ac.in.

(1) Collman, J. P.; Wagenknecht, P. S.; Hutchison, J. E. *Angew. Chem., Int. Ed. Engl.* **1994**, *33*, 1537.

(2) (a) Beletskaya, I.; Tyurin, V. S.; Tsivadze, A. Y.; Guilard, R.; Stern, R. *Chem. Rev.* **2009**, *109*, 1659. (b) Harvey, P. D.; Stern, C.; Gros, C. P.; Guilard, R. *Coord. Chem. Rev.* **2007**, *251*, 401. (c) Rosenthal, J.; Nocera, D. G. *Acc. Chem. Res.* **2007**, *40*, 543. (d) Rosenthal, J.; Bachman, J.; Dempsey, J. L.; Esswein, A. J.; Gray, T. G.; Hodgkiss, J. M.; Manke, D. R.; Luckett, T. D.; Pistorio, B. J.; Veige, A. S.; Nocera, D. G. *Coord. Chem. Rev.* **2005**, *249*, 1316.

(3) (a) Rosenthal, J.; Luckett, T. D.; Hodgkiss, J. M.; Nocera, D. G. *J. Am. Chem. Soc.* **2006**, *128*, 6546. (b) Rosenthal, J.; Pistorio, B. J.; Chng, L. L.; Nocera, D. G. *J. Org. Chem.* **2005**, *70*, 1885. (c) Chang, C. J.; Loh, Z.-H.; Deng, Y.; Nocera, D. G. *Inorg. Chem.* **2003**, *42*, 8262. (d) Hodgkiss, J. M.; Chang, C. J.; Pistorio, B. J.; Nocera, D. G. *Inorg. Chem.* **2003**, *42*, 8270. (e) Chang, C. J.; Baker, E. A.; Pistorio, B. J.; Deng, Y.; Loh, Z.-H.; Miller, S. E.; Carpenter, S. D.; Nocera, D. G. *Inorg. Chem.* **2002**, *41*, 3102. (f) Loh, Z.-H.; Miller, S. E.; Chang, C. J.; Carpenter, S. D.; Nocera, D. G. *J. Phys. Chem. A* **2002**, *106*, 11700. (g) Pistorio, B. J.; Chang, C. J.; Nocera, D. G. *J. Am. Chem. Soc.* **2002**, *124*, 7884.

(4) (a) Clement, T. E.; Nurco, D. J.; Smith, K. M. *Inorg. Chem.* **1998**, *37*, 1150. (b) Medforth, C. J.; Hobbs, J. D.; Rodriquez, M. R.; Abraham, R. J.; Smith, K. M.; Shelnutt, J. A. *Inorg. Chem.* **1995**, *34*, 1333. (c) Senge, M. O.; Gerzevske, K. R.; Vicente, M. G. H.; Forsyth, T. P.; Smith, K. M. *Angew. Chem., Int. Ed. Engl.* **1993**, *32*, 750.

© 2010 American Chemical Society Published on Web 03/10/2010

Scheme 1

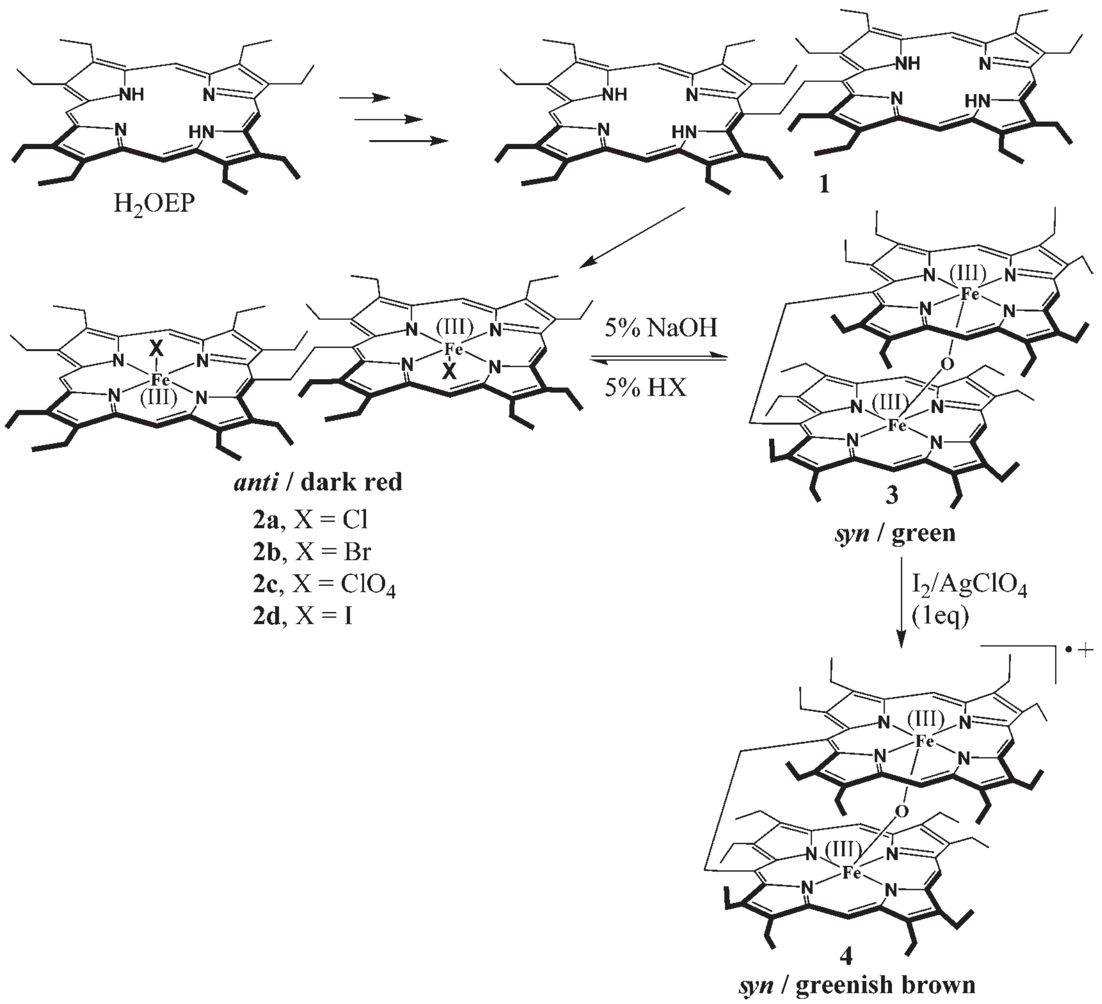

enhancing oxidation owing to greater substrate access for activation and subsequent reaction.[1−3] In light of the proven effectiveness of the functioning of such bisporphyrin molecules, we undertook to evaluate the structure, properties, and function of bis(iron(III) octaethylporphyrin) containing highly flexible ethane as linker. We have synthesized and structurally characterized *anti*-bis-Fe(III) porphyrins with axial ligand X (X: Cl, Br, I, ClO$_4$) which stabilizes the *anti* form of the molecule. Upon treatment with base, the molecule converts remarkably bent bisFe(III)-μ-oxo porphyrins in its *syn* form. The facile *syn*-*anti* transformation demonstrates the unprecedented ability of the bisporphyrin platforms to "open" and "close" its binding pockets reversibly in a single molecular framework. We have recently reported briefly the X-ray structure and some of the reactivity of the bisFe(III)-μ-oxo porphyrin as a preliminary communication.[7]

Results and Discussion

The free ligands H$_2$OEP[9a] and 1,2-bis(*meso*-octaethylporphyrinyl)ethane, **1**,[9b] and 1,2-bis[Chloroiron(III) octaethylporphyrinyl]ethane, **2a**,[8b] have been synthesized after some modifications of the reported procedures. In a degassed solvent mixture of CH_3CN and $CHCl_3$ (2:1), **1** was treated with $FeBr_2$ at 55 °C for 40 min under N_2 atmosphere which upon aerial oxidation yields 1,2-bis[bromoiron(III) octaethylporphyrinyl)ethane, **2b**, in excellent yields. 1,2-Bis[perchloratoiron(III) octaethylporphyrinyl)ethane, **2c**, is prepared by the treatment of **2a** in benzene with $AgClO_4$; the dark crystalline solid of the molecule deposited in high yields via slow diffusion of hexanes into the dichloromethane solution of the complex. The axial ClO_4^- of **2c** can also be replaced by I^- using aqueous KI to produce 1,2-bis[iodoiron(III) octaethyl porphyrinyl]ethane, **2d**, in excellent yields. Scheme 1 shows the synthetic strategy and molecular structures of all the complexes reported in the paper and their abbreviations.

---

(5) (a) Frampton, M. J.; Akdas, H.; Cowley, A. R.; Rogers, J. E.; Slagle, J. E.; Fleitz, P. A.; Drobizhev, M.; Rebane, A.; Anderson, H. L. *Org. Lett.* **2005**, *7*, 5365. (b) Setsune, J.-I.; Takeda, H.; Ito, S.; Saito, Y.; Ishimaru, Y.; Fukuhara, K.; Saito, Y.; Kitao, T.; Adachi, T. *Inorg. Chem.* **1998**, *37*, 2235.

(6) (a) Takai, A.; Gros, C. P.; Barbe, J.-M.; Guilard, R.; Fukuzumi, S. *Chem.—Eur. J.* **2009**, *15*, 3110. (b) Borovkov, V. V.; Fujii, I.; Muranaka, A.; Hembury, G. A.; Tanaka, T.; Ceulemans, A.; Kobayashi, N.; Inoue, Y. *Angew. Chem., Int. Ed.* **2004**, *43*, 5481. (c) Fletcher, J. T.; Therien, M. J. *Inorg. Chem.* **2002**, *41*, 331. (d) Sugiura, K.-I.; Ponomarev, G. V.; Okubo, S.; Tajiri, A.; Sakata, Y. *Bull. Chem. Soc. Jpn.* **1997**, *70*, 1115.

(7) Ghosh, S. K.; Patra, R.; Rath, S. P. *Inorg. Chem.* **2008**, *47*, 10196.

(8) (a) Hembury, G. A.; Borovkov, V. V.; Lintuluoto, J. M.; Inoue, Y. *Chem. Lett.* **2003**, *32*, 428. (b) Borovkov, V. V.; Lintuluoto, J. M.; Inoue, Y. *Helv. Chim. Acta* **1999**, *82*, 919. (c) Hitchcock, P. B. *J. Chem. Soc., Dalton Trans.* **1983**, 2127.

(9) (a) Sessler, L. J.; Mozaffari, A.; Johnson, M. R. *Org. Synth.* **1992**, *70*, 68. (b) Arnold, D.; Johnson, A. W.; Winter, M. *J. Chem. Soc., Perkin Trans. 1* **1977**, 1643.

UV−visible spectroscopy is particularly useful to determine the geometry of the metal-bisporphyrin complex in solution. The splitting of the Soret band was often observed for various porphyrin dimers and trimers in linear spatial orientations.[10] For example, a split in the Soret band was found for the *anti* conformation of bis(Zinc porphyrin) in the presence of external ligands as a result of coordination to the Zinc ions.[10a,d] Similar splitting in the Soret band was also observed for **2c** which shows two well resolved $B_\perp$ and $B_\parallel$ transitions at 390 and 410 nm in dichloromethane and thus is clearly indicative of *anti* conformation in solution. The *anti* conformation of the molecule is also observed in the solid state X-ray structure (vide infra). Similar UV−vis spectral patterns are also observed for **2a**, **2b**, and **2d** which suggests the presence of *anti* conformation for the molecules.

However, dichloromethane solution of **2** while shaking with a 5% NaOH solution immediately changes color from dark red to green because of the formation of bis Fe(III)-μ-oxo porphyrin, **3**, which was isolated in pure form after chromatographic separation in excellent yields and also structurally characterized. UV−vis spectroscopic data for **3** (Soret band at 402 nm and Q-band at 579 nm in benzene) suggest the face-to-face orientation of the porphyrin macrocycles in solution which is also authenticated in the X-ray structure of the molecule (vide infra). However, **3** can easily be transformed in solution to **2** again by adding the appropriate acid, HX. The facile *syn*-*anti* conformational switching between **2** and **3** are reversible with sharp change in color and found to be acid−base controlled. Figure 1 shows the UV−vis spectra of **3** and **2c** in its *syn* and *anti* form, respectively. One-electron oxidation of μ-oxo complex, **3**, is performed using both chemical and electrochemical methods, and the progress of the oxidations is also monitored in solution using ^{1}H NMR spectroscopy (vide infra).

Crystallographic Characterization of 2c. The molecule crystallizes via slow evaporation of the chloroform solution of the complex in the monoclinic crystal system with $P2_1$ space group. A perspective view is shown in Figure 2, and the selected bond distances and angles are given in Table 1. The complex has two iron centers each in a five coordinate square-pyramidal geometry and is in *anti* conformations. The iron atoms are displaced by 0.44 and 0.42 Å from the N4 planes of core-I and II, respectively, a distance which is in the range of 0.39−0.54 Å seen for other high-spin (*S*, 5/2) five-coordinate iron(III) porphyrins.[11] There is a considerable distortion from planarity of the porphyrin rings as can be seen in Figure 2. In particular, the bridging *meso* carbons, namely C20 and C120, are considerably out of the mean plane. This is presumably to minimize the nonbonded contact between the two rings, and the Fe···Fe distance is 10.04 Å. However, there are only two structural reports with ethane bridged bis porphyrin **1**; in one it exist as the *anti* form with a Ni···Ni separation of 9.93 Å[8c] whereas in the other it stabilizes *tweezer*-type structures where the Zn···Zn separation is 5.604(5) Å.[6b]

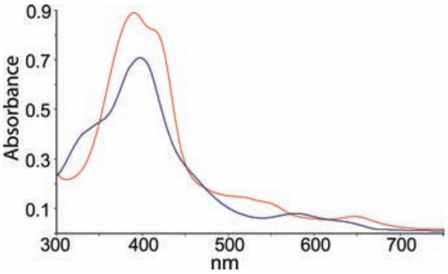

Figure 1. UV−visible spectra in benzene for **2c** (red line) and **3** (blue line) at 295 K.

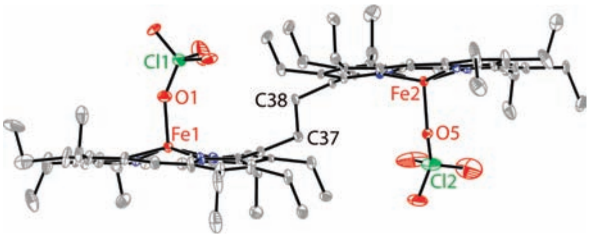

Figure 2. Perspective view of **2c** showing 50% thermal contours for all non-hydrogen atoms at 100 K (H-atoms have been omitted for clarity).

Table 1. Selected Bond Lengths (Å) and Bond Angles (deg) for **2c**, **3a**, and **3b**

	2c	**3a**	**3b**
Fe1−O1	1.873(9)	1.779(2)	1.769(2)
Fe1−N1	2.059(10)	2.068(3)	2.081(3)
Fe1−N2	2.051(9)	2.060(3)	2.080(3)
Fe1−N3	2.039(9)	2.076(3)	2.073(3)
Fe1−N4	2.097(9)	2.069(3)	2.075(3)
Fe2−O5	1.940(7)	1.768(2)	1.766(2)
Fe2−N101	2.031(9)	2.075(3)	2.068(3)
Fe2−N102	2.053(8)	2.080(3)	2.070(3)
Fe2−N103	2.081(9)	2.069(3)	2.084(3)
Fe2−N104	2.061(9)	2.067(3)	2.077(3)
C37−C38	1.511(14)	1.546(5)	1.554(5)
O1−Fe1−N1	105.2(4)	99.60(11)	108.44(11)
O1−Fe1−N2	99.0(4)	102.07(11)	107.82(11)
O1−Fe1−N3	101.2(4)	107.39(11)	100.50(11)
O1−Fe1−N4	104.4(4)	108.84(11)	98.61(11)
O5−Fe2−N101	102.2(3)	106.81(11)	101.96(11)
O5−Fe2−N102	101.3(3)	106.63(11)	101.48(12)
O5−Fe2−N103	103.0(4)	101.75(12)	105.98(11)
O5−Fe2−N104	100.7(3)	102.92(11)	106.64(11)
N1−Fe1−N2	87.8(4)	88.04(11)	87.36(11)
N1−Fe1−N3	153.6(4)	153.01(11)	150.97(11)
N1−Fe1−N4	85.6(4)	84.84(11)	84.84(11)
N2−Fe1−N3	86.3(4)	85.91(12)	85.88(11)
N2−Fe1−N4	156.5(4)	149.02(11)	153.56(11)
N3−Fe1−N4	89.7(3)	86.92(11)	88.79(11)
N101−Fe2−N102	86.0(4)	87.12(11)	88.56(11)
N101−Fe2−N103	154.7(4)	151.44(12)	152.05(11)
N101−Fe2−N104	89.4(3)	84.90(11)	84.97(11)
N102−Fe2−N103	88.0(3)	85.22(11)	85.24(11)
N102−Fe2−N104	158.0(3)	150.44(11)	151.87(12)
N103−Fe2−N104	87.1(3)	88.33(11)	87.77(11)

Figure 3 shows the packing diagram of **2c** which also shows the $\pi-\pi$ interactions (with 3.683(6) Å separation) between the pyrrole rings of the two adjacent molecules. Table 2 compares all structurally characterized five-coordinate iron(III) porphyrins reported[12] so far using ClO_4

---

[10] (a) Borovkov, V. V.; Hembury, G. A.; Yamamoto, N.; Inoue, Y. *J. Phys. Chem. A* **2003**, *107*, 8677. (b) Higuchi, H.; Shinbo, M.; Usuki, M.; Takeuchi, M.; Keita, T.; Yamamoto, K. *Bull. Chem. Soc. Jpn.* **2000**, *73*, 1259. (c) Higuchi, H.; Shinbo, M.; Usuki, M.; Takeuchi, M.; Hasegawa, Y.; Tani, K.; Ojima, J. *Bull. Chem. Soc. Jpn.* **1999**, *72*, 1887. (d) Borovkov, V. V.; Lintuluoto, J. M.; Inoue, Y. *J. Phys. Chem. B* **1999**, *103*, 5151.

[11] Scheidt, W. R. In *The Porphyrin Handbook*; Kadish, K. M., Smith, K. M., Guilard, R., Eds.; Academic Press: San Diego, CA, 2000; Vol. *3*, p 49.

[12] (a) Barkigia, K. M.; Renner, M. W.; Fajer, J. *J. Porphyrins Phthalocyanines.* **2001**, *5*, 415. (b) Oyaizu, K.; Haryono, A.; Natori, J.; Shinoda, H.; Tsuchida, E. *Bull. Chem. Soc. Jpn.* **2000**, *73*, 1153. (c) Masuda, H.; Taga, T.; Osaki, K.; Sugimoto, H.; Yoshida, Z.-I.; Ogoshi, H. *Inorg. Chem.* **1980**, *19*, 950. (d) Reed, C. A.; Mashiko, T.; Bentley, S. P.; Kastner, M . E.; Scheidt, W. R.; Spartalian, K.; Lang, G. *J. Am. Chem. Soc.* **1979**, *101*, 2948.

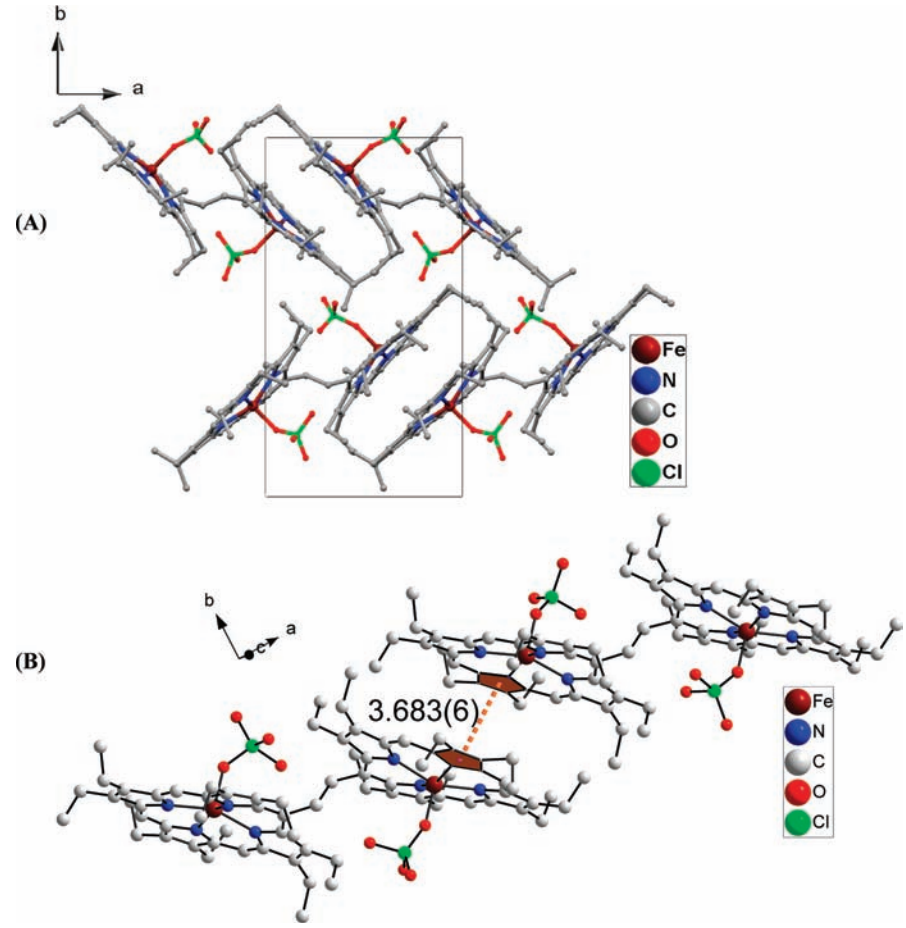

Figure 3. (A) Diagram illustrating the packing of the **2c** molecules in the unit cell. (B) Diagram illustrating the $\pi-\pi$ interaction between two **2c** molecules.

Table 2. Selected Structural Parameters for Fe^{III}(porphyrin)ClO_4 Core

complex		$Fe-N_p$[a]	$Fe-O$[a]	Δ^{Fe}_{4N}[b]	Δ_{24}[c]	C_m[d]	C_β[e]	spin state	ref
Fe^{III}(OEP)ClO_4		1.994(10)	2.067(9)	0.26	0.03	0.02	0.04	intermediate (*S*, 3/2)	12c
Fe^{III}(TPP)ClO_4		2.001(4)	2.029(4)	0.28	0.13	0.18	0.18	admixed IS	12d
Fe^{III}(TPP)ClO_4		2.009(4)	2.042(6)	0.28	0.11	0.20	0.10	admixed IS	12b
Fe^{III}(OETPP)ClO_4		1.963	2.059	0.26	0.65	0.19	1.32	intermediate (*S*, 3/2)	12a
2c	Core-I	2.062(9)	1.873(9)	0.44	0.11	0.16	0.15	high spin (*S*, 5/2)	tw
	Core-II	2.057(9)	1.940(7)	0.42	0.11	0.13	0.15		

[a] Average value in Å. [b] Displacement of iron from mean plane containing four porphyrinic nitrogen. [c] Average displacement of the 24 atoms from the least-squares plane of the porphyrin. [d] Average displacement of *meso* carbons from mean plane containing 24 porphyrin atoms. [e] Average displacement of *beta*-carbons from the mean porphyrin plane (24 atoms).

as axial ligand along with our molecule, **2c**. As can be seen from the table, the average Fe−Np distances of 2.062(9) (core-I) and 2.057(9) Å (core-II) for **2c** are longest compared to all other complexes while the corresponding Fe−O distances of 1.873(9) and 1.940(7) Å are also shortest in the series. To compare, the mean Fe−Np and Fe−$OClO_3$ bond lengths are 1.994(10) and 2.067(9) Å, respectively, in the case of Fe^{III}(OEP)ClO_4. The core size is also largest for **2c** compared to all other five-coordinated porphyrins using ClO_4 as axial ligand.

The EPR spectral measurements are carried out for **2** at 110 K both in solid and solution phase, and three of them are also shown in Figure 4. All the spectra are axially symmetric with $g_\perp = 5.98$ and $g_\| = 1.99$ for **2a**; $g_\perp = 5.97$ and $g_\| = 1.99$ for **2b**; $g_\perp = 5.95$ and $g_\| = 2.00$ for **2c**; and $g_\perp = 5.96$ and $g_\| = 1.99$ for **2d** in dichloromethane. Very similar *g* values are also obtained for the molecules in the solid phase (see Experimental Section, vide infra). These results provide unequivocal evidence of high spin Fe(III) ($S = 5/2$) nature of the complexes both in solid and solution phase.[13]

The ^1H NMR spectra of complex **2** are shown in Figure 5. Since there is a C_2 axis of symmetry in **2**, ^1H NMR resonance pattern should be similar with *meso*-substituted five-coordinate Fe porphyrins of type XFe^{III}-(*meso*-R-OEP).[14] It is thus expected that there should be

---

[13] (a) Walker, F. A. *Chem. Rev.* **2004**, *104*, 589. (b) Walker, F. A. *Coord. Chem. Rev.* **1999**, *186*, 471. (c) Nakamura, M.; Ohgo, Y.; Ikezaki, A. *J. Inorg. Biochem.* **2008**, *102*, 433. (d) Nakamura, M. *Coord. Chem. Rev.* **2006**, *250*, 2271.

[14] (a) Kalish, H.; Camp, J. E.; Stepien, M.; Latos-Grażyński, L.; Olmstead, M. M.; Balch, A. L. *Inorg. Chem.* **2002**, *41*, 989. (b) Balch, A. L.; Latos-Grażyński, L.; Noll, B. C.; Olmstead, M. M.; Zovinka, E. P. *Inorg. Chem.* **1992**, *31*, 2248.

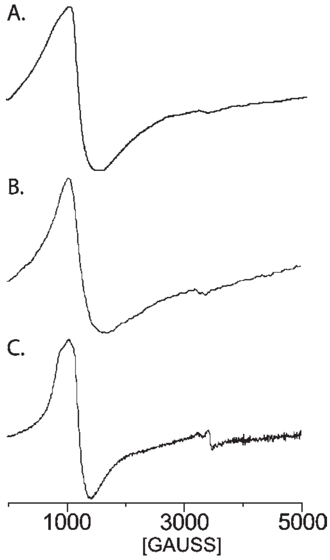

Figure 4. X-band EPR spectra in CH_2Cl_2 (at 110 K) of **2a** (A), **2b** (B), and **2c** (C).

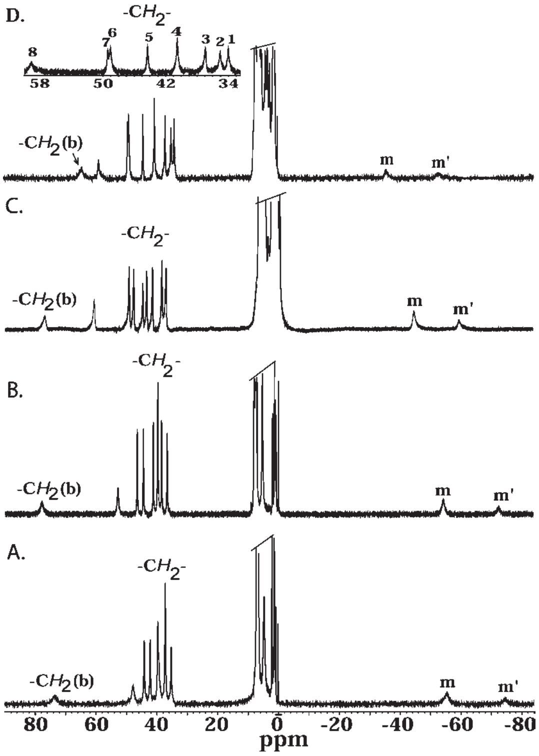

Figure 5. ^1H NMR spectra in $CDCl_3$ at 295 K (A) **2a**, (B) **2b**, (C) **2d**, and (D) **2c**.

two *meso* resonances in a 2:1 intensity ratio, eight methylene resonances, and four equally intense methyl resonances for five-coordinate complex, **2**. The eight methylene resonances arise from the diastereotopic nature of these protons which occurs whenever the two sides of the porphyrin are inequivalent. As seen in Figure 5, there are two resonances in the far upfield region with a 2:1 intensity ratio that can be assigned to the *meso* protons, and eight resonances (~40 ppm) in the downfield region that can be assigned to the methylene protons. However, the bridging $-CH_2$- shows only one resonance at the most downfield region. As expected, the resonances for methyl protons are found in the narrow diamagnetic window from 0 to 10 ppm since they are far off from the metal center. For example, the ^1H NMR spectrum of **2a** in $CDCl_3$ (after passing through basic alumina) at 295 K is broad, and eight diastereotopic methylene proton signals comes at 35.3, 37.2, 39.7, 42.2, 44.1, 44.5, and 48.1 ppm, two *meso* resonances at −74.7 and −55.0 ppm in 1:2 ratios while the bridging ethylene signal comes at 73.5 ppm. By changing the axial ligations from Cl^- to Br^- to I^- and then ClO_4^-, two *meso* and eight methylene proton signals gradually move downfield while the bridging CH_2- signals move more and more upfield. It is also interesting to note that the methylene proton signals are spread out gradually in the same direction. Resonance assignments have been made on the basis of relative intensities and line widths. The temperature dependence of the signals almost follows the Curie law as shown in Figure 6 indicative of a single spin state throughout the temperature range. Also, the positioning of the methylene and *meso* signals provides unequivocal evidence for the high spin (S = 5/2) nature of **2** in solution phase.

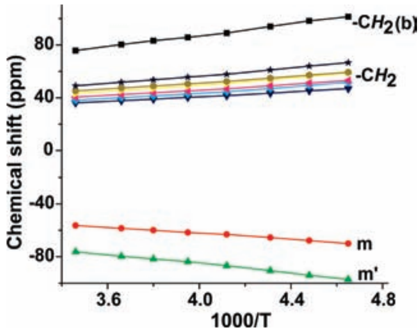

Figure 6. Curie plot (chemical shift versus $1/T$) of the proton signals for **2a**.

The magnetic moment (and also χT) of the polycrystalline samples of **2b** is found substantially independent of temperature over the temperature range from 5 to 300 K; Figure 7 shows the plot of the effective magnetic moment against the temperature. The effective magnetic moment is found to be 5.86 μ_B per iron at 295 K, which further confirms the high-spin nature of the complex. Similar magnetic behaviors are also observed for other Fe(III) complexes reported here. Solution magnetic moments at 295 K in the purified dichloromethane, calculated by the modified Evan's method,[15] are found to be 5.81, 5.91, 5.78, and 5.88 BM per iron center for **2a**, **2b**, **2c**, and **2d**, respectively, which are again very close to the values obtained in the crystalline states and are very characteristics of the high-spin nature (S = 5/2) of the complexes.

Several factors control the spin states of iron(III) porphyrin complex. Among these, the number and nature of axial ligands are the most important factors. While most of the anionic ligands such as halides and hydroxide lead to the formation of the complexes with high-spin (S = 5/2) state, extremely weak ligands such as ClO_4^- and SbF_6^- give invariably the admixed (S = 3/2, 5/2) spin state.[16,17] Fajer and co-workers have also reported that five-coordinated Fe^{III}(OETPP)ClO_4 is an essentially pure S = 3/2 complex on the basis of the EPR and crystallographic studies.[12a] Table 2 compares the structure and

---

(15) Sur, S. K. *J. Magn. Reson.* **1989**, *82*, 169.

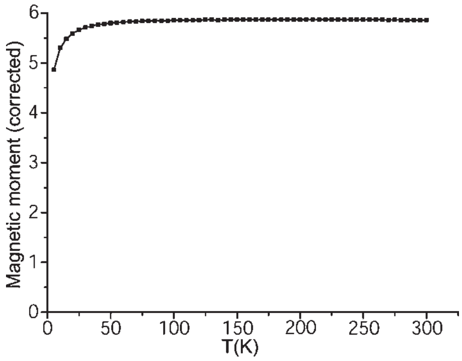

Figure 7. Magnetic moment per iron center of crystalline sample of **2b** as a function of temperature.

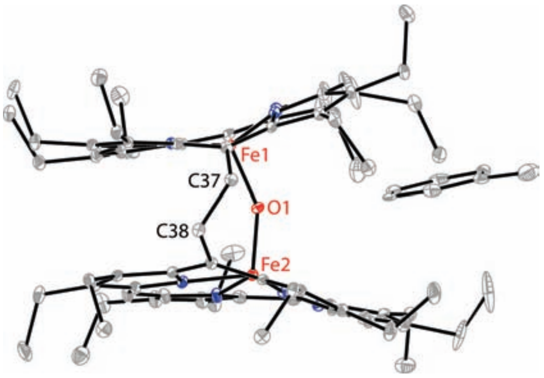

Figure 8. Perspective view of **3b** showing 50% thermal contours for all non-hydrogen atoms at 100 K (H-atoms have been omitted for clarity).

geometrical features of all Fe^{III}(porphyrin)ClO_4 complexes reported here and elsewhere; our molecule **2c** only authenticates the "pure" high-spin nature of the complex in both solid and solution phase. In contrast, all reported Fe^{III}(por)ClO_4 complexes have either admixed or "pure" intermediate spin states of iron.[12]

The complex **3** crystallizes as two different solvates: **3a** (with CH_3CN) and **3b** (with toluene) grown from two different solvent combinations and reported briefly in a communication.[7] Both of them crystallize in the monoclinic crystal system with very similar structure and bonding parameters. A perspective view of **3b** is shown in Figure 8, and the selected bond distances and angles are given in Table 1. The average Fe−O and Fe−N bond lengths in **3** are normal for any iron(III)μ-oxo porphyrin dimers. However, Fe−Np distances increase from **2c** to **3** while Fe−O distances decreases significantly in the same directions although both are five-coordinate. The most striking feature of the structure in **3** is the remarkably bent Fe−O−Fe unit with angles of 147.9(1)° for **3a** and 151.1(1)° for **3b**. The structure of **3** (Figure 8) clearly demonstrates the dramatic ability of bisporphyrin **1** to "bite" down on exogenous ligands and, as a result, the Fe···Fe distance which was 10.04 Å in **2c** is now reduced to 3.409(1) Å for **3a**. A comparative structural analysis between **2c** and **3** has shown the unique ability of this platform to "open" and "close" its binding pocket with very high vertical flexibility of over 6.5 Å.

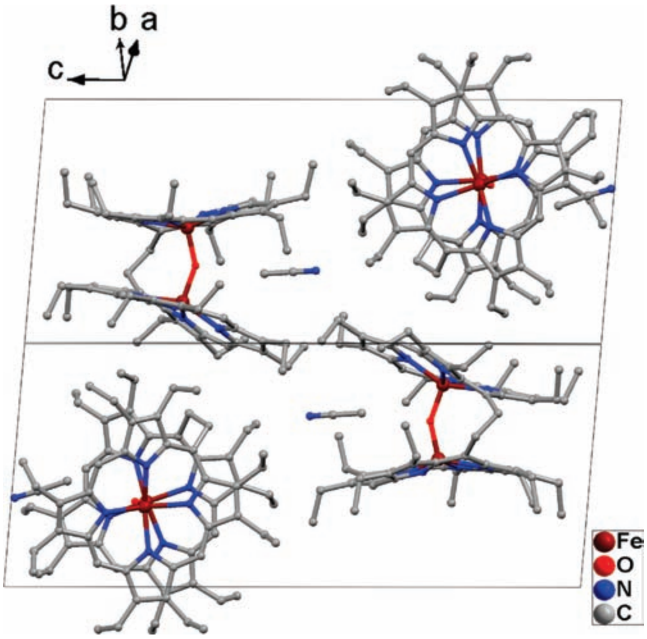

Figure 9. Diagram illustrating the packing of the **3a** molecules in the unit cell.

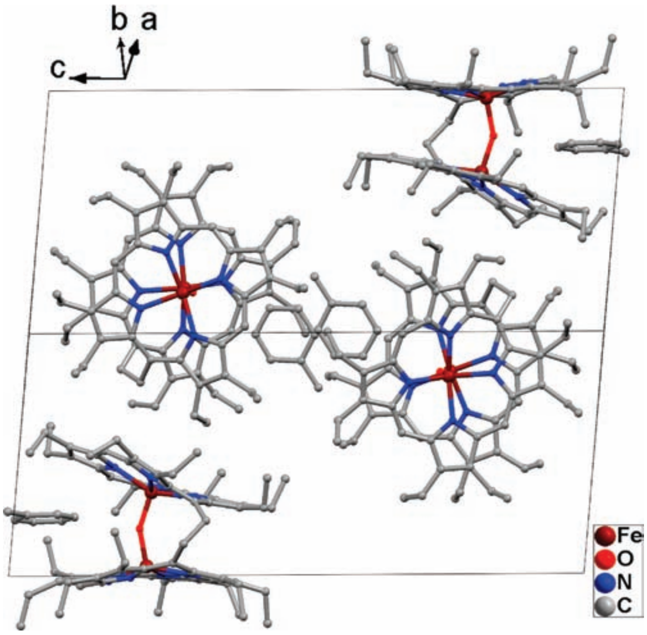

Figure 10. Diagram illustrating the packing of the **3b** molecules in the unit cell.

Figures 9 and 10 show the packing diagrams of **3a** and **3b**, respectively, in which the solvent molecules (CH_3CN for **3a** and toluene for **3b**) are wedged into the opening between two rings and are stabilized by CH−π and π−π interaction respectively with the rings. Similar stabilization of the substrates by the rings could be anticipated

---

(16) Weiss, R.; Gold, A.; Terner, J. *Chem. Rev.* **2006**, *106*, 2550.

(17) (a) Sakai, T.; Ohgo, Y.; Hoshino, A.; Ikeue, T.; Saitoh, T.; Takahashi, M.; Nakamura, M. *Inorg. Chem.* **2004**, *43*, 5034. (b) Sakai, T.; Ohgo, Y.; Ikeue, T.; Takahashi, M.; Takeda, M.; Nakamura, M. *J. Am. Chem. Soc.* **2003**, *125*, 13028. (c) Nakamura, M.; Takahisa, I.; Ohgo, Y.; Takahashi, M.; Takeda, M. *Chem. Commun.* **2002**, 1198. (d) Ikeue, T.; Ohgo, Y.; Yamaguchi, T.; Takahashi, M.; Takeda, M.; Nakamura, M. *Angew. Chem., Int. Ed.* **2001**, *40*, 2617. (e) Ikeue, T.; Saitoh, T.; Yamaguchi, T.; Ohgo, Y.; Nakamura, M.; Takahashi, M.; Takeda, M. *Chem. Commun.* **2000**, 1989. (f) Nesset, J. M.; Cai, S.; Shokhireva, T. K.; Shokhirev, N. V.; Jacobson, S. E.; Jayaraj, K.; Gold, A.; Walker, F. A. *Inorg. Chem.* **2000**, *39*, 532. (g) Reed, C. A.; Guiset, F. *J. Am. Chem. Soc.* **1996**, *118*, 3281. (h) Boersma, A. D.; Goff, H. M. *Inorg. Chem.* **1982**, *21*, 581. (i) Goff, H.; Shimomura, E. *J. Am. Chem. Soc.* **1980**, *102*, 31.

Table 3. Selected Geometrical Parameters

complex	Fe−N$_p$[a]	Fe−O[a]	Fe−O−Fe (°)	Fe···Fe[a]	$\Delta^{Fe}{}_{24}$[b]	Δ_{24}[c]	MPS[d]	Φ[e]	Θ[f]	ref
$Fe_2(\mu\text{-}O)FF.H_2O$	2.075(7)	1.787(6)	161.1(4)	3.525	0.62	0.12	4.71	24.25	15.8	19e
Fe_2O(DPD)	2.104	1.782	158.7	3.504	0.66	0.17	4.68	1.55	21.8	19d
Fe_2O(DPXM)	2.087(4)	1.789(3)	155.2	3.493	0.70	0.28	4.74	3.7	25.4	19a
Fe_2O(DPA)	2.0849(2)	1.7593(3)	165.729(8)	3.491	0.49	0.04	4.45	0.7	10.1	19b
Fe_2O(DPX)	2.0836(4)	1.7575(3)	174.808(8)	3.511	0.50	0.07	4.49	2.94	1.2	19c
3a	2.070(3)	1.774(2)	147.9(1)	3.409	0.57	0.20	4.33	16.1	25	7
3b	2.076(3)	1.767(2)	151.1(1)	3.423	0.54	0.18	4.3	16.4	21.2	7

[a] Average value in angstrom. [b] Displacement of iron from mean plane containing 24 porphyrin atoms. [c] Average displacement of the 24 atoms from the least-squares plane of the porphyrin. [d] Average distance of two least-squares plane of the porphyrin (24 atoms). [e] Average of the four N−Fe−Fe'−N' dihedral angles. [f] Angle between the two least-squares planes (24 atom).

which could be responsible for the selectivity and efficiency of the catalytic processes in the so-called "Pac-Man" systems. The close approach of the two porphyrin rings leads to a core deformation with an average deviations of 0.20 (for **3a**) and 0.18 Å (for **3b**) from the mean porphyrin plane (of 24 atoms) while the *meso* carbons that are connected through the bridging ligands are displaced most. The two porphyrin cores in both molecules are structurally inequivalent in the solid state; a curious feature is that the core-I is much more distorted than the core-II. The two cores are not parallel with respect to each other; in fact, half of the cores are nearly coplanar (dihedral angles are 5.3° and 5.6° for **3a** and **3b**) with ~3.7 Å separation while the other half makes a dihedral angles of 45.7° and 38.0° for **3a** and **3b**, respectively. However stabilization out of the $\pi-\pi$ interaction in **3** is highly unlikely due to face-to-face alignment of the two rings.[18] The relative orientations of the two porphyrin rings are such as to make torsional angles of 16.1° for **3a** and 16.4° for **3b** while the interplanar angles are 25° and 21.2°, respectively.

Table 3 compares the geometrical features of all the structurally characterized diiron(III)-μ-oxobisporphyrins reported[19] in the literature along with **3a** and **3b**. As can be seen, the Fe−N distances for **3** are shortest in the series while the Fe−O distances are all very similar. The Fe···Fe non bonding distances are found to be 3.409(1) Å for **3a** and 3.423(1) Å for **3b**; the values are also nearly 0.1 Å shorter compared to the similar distances observed in other μ-oxo dimer. As can be seen in Table 3, the Fe−O−Fe angle of 147.9(1)° for **3a** authenticates the smallest angle in the series. For comparison, the two smallest Fe−O−Fe angles reported so far for any co-facial bisporphyrinic μ-oxo dimers are one for dibenzofuran-bridged co-facial bisporphyrin (158.7°)[19d] and another one for diporphyrin xanthene methoxyaryl oxo-bridged dimer (155.2°).[19a]

The porphyrin rings are highly distorted in the complexes reported here and are best appreciated by turning to Figure 11 where the out-of-plane displacements in units of 0.01 Å of the porphyrin core atoms are compared. As can be seen, the rings in **3** are much more distorted compared to **2c**. The nomenclature that describes the types of distortions commonly observed in nonplanar porphyrins was originally suggested by Scheidt and Lee.[20] In a saddle conformation, alternate pyrrole rings tilt up and down with respect to the porphyrin mean plane (24 atoms), and the *meso* carbon atoms lie on the least-squares plane. In a ruffled conformation, alternate pyrrole rings twist clockwise or counterclockwise about the metal nitrogen bond, and the *meso* carbon atoms move alternately above or below the least-squares plane of the 24 porphyrin atom core. As is evident from Figure 11, the ring distortions of **3** can be described as the ruffle type with alternating displacements of the pyrrole rings below and above the mean porphyrin plane. However, the rings in **2c** have significant saddle conformations. Shelnutt et al

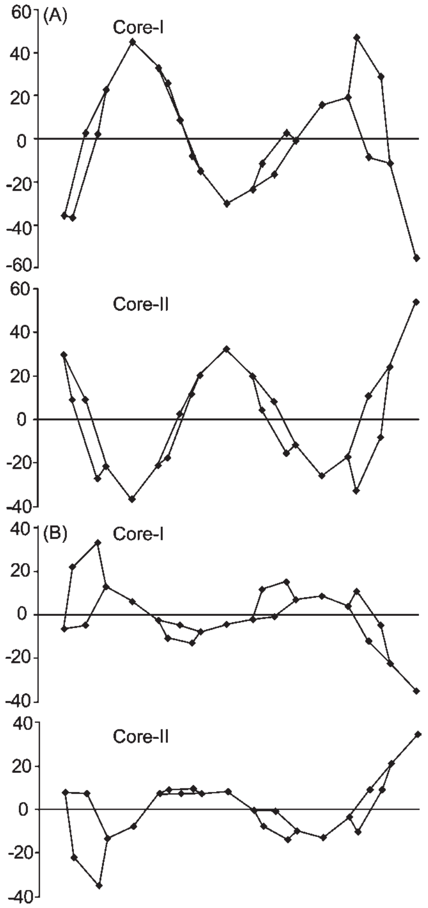

Figure 11. Out-of-plane displacements (in units of 0.01 Å) (A) for **3a**, (B) for **2c** of the porphyrin core atoms from the mean porphyrin plane (24 atoms).

---

(18) (a) Janiak, C. *J. Chem. Soc., Dalton Trans.* **2000**, 3885. (b) Hunter, C. A.; Sanders, J. K. M. *J. Am. Chem. Soc.* **1990**, *112*, 5525.

(19) (a) Chang, C. J.; Loh, Z.-H.; Shi, C.; Anson, F. C.; Nocera, D. G. *J. Am. Chem. Soc.* **2004**, *126*, 10013. (b) Lee, G.-H. Private Communication **2003** (CCDC 115142). (c) Lee, G.-H. Private Communication **2003** (CCDC 115144).(d) Deng, Y.; Chang, C. J.; Nocera, D. G. *J. Am. Chem. Soc.* **2000**, *122*, 410. (e) Landrum, J. T.; Grimett, D.; Haller, K. J.; Scheidt, W. R.; Reed, C. A. *J. Am. Chem. Soc.* **1981**, *103*, 2640.

(20) Scheidt, W. R.; Lee, Y. J. *Struct. Bonding* (*Berlin*) **1987**, *64*, 1.

have developed a normal coordinate structural decomposition method (NSD)[21] which simulates any porphyrin distortion by a linear combinations of six normal deformations; saddled (sad), ruffled (ruf), domed (dom), wav(x), wav(y), and propeller (pro), and also yields total out-of plane displacements (*D*oop). The results of NSD analysis of the complexes are presented in Table S1 (see Supporting Information).

To understand why **3** prefers such a bent geometry, we first compare it with [Fe(OEP)]$_2$O in which the Fe−O−Fe bond angles are 176.2° (for monoclinic) and 172.2° (for triclinic).[22a] The same molecule while crystallizing with C_{60} in benzene forms co-crystal $C_{60}\cdot$[Fe(OEP)]$_2$O$\cdot C_6H_6$ with benzene molecule wedged into the opening between two rings, and Fe−O−Fe angles are found to be ~151°.[22b] In the hydroxo bridged [Fe(OEP)]$_2$(OH)$\cdot ClO_4$ complex, the Fe−O(H)−Fe angle is 146.2°.[22c] Two Fe−O(H) distances of 1.924(3) and 1.952(3) Å are significantly longer resulting relatively longer Fe$\cdots$Fe nonbonding distance (3.707 Å) and electronic effect at oxygen contributes significantly in the bending of Fe−O(H)−Fe unit. Molecular mechanics calculations of Shelnutt, Scheidt, and co-workers predicted that a dimer with all ethyl groups on the "outside" would have an Fe−O−Fe angle of 155.2°, and the core makes a 32.2° twist angle to minimize the ethyl group interactions.[22a] In contrast, the rings in **3a** and **3b** are nearly eclipsed with even lower Fe−O−Fe angles and that too with 4 (out of 16) ethyl group in the "inward" direction. Also, two rings in **3** are not slipped (deemed group S,[20] small lateral shifts) but face to face in a nearly eclipsed geometry while half of the rings are almost parallel with ~3.7 Å interplanar separations. However, the observed Fe−O−Fe angles of 147.9(1) Å for **3a** and 151.1(1) Å for **3b** are such that at least six carbon atoms at the periphery from each of the macrocycles are driven to be essentially less than the van der Waals contact distance. To a significant extent, the bending is promoted by the "outward" direction of the peripheral ethyl groups as well as the positioning of solvent molecule in between the rings for all these cases.

Variable temperature magnetic susceptibility measurements have been carried out for **3** also between 5 and 350 K, the plot of μ_{eff} versus T is shown in Figure 12. The magnetic moments decrease from 2.65 μ_B at 350 K with a decrease of the temperature and reach a plateau at about 60 K, which is consistent for strong antiferromagnetically coupled $S = 5/2$ pairs. The $\chi_M T$ versus T data have been subjected to a least-squares fit ($-J$, 126.6 cm^{-1}) to the expression derived from the spin Hamiltonian $H = -2JS_1S_2$, where $S_1 = S_2 = 5/2$. Also **3** does not show any electron paramagnetic resonance (EPR) signal either in the solid or in solution (110 K), consistent with strong antiferromagnetic couplings between the two high-spin iron(III) centers. The ^{1}H NMR spectrum of **3** in $CDCl_3$ (after passing through basic alumina) at 295 K is broad, and the *syn* orientation is preserved in solution as evidenced by the presence of eight diastereotopic methylene protons at 6.4, 6.3, 6.1, 5.9, 5.5, 5.2, 5.1, and 5.0 ppm, two *meso* resonances at 4.8 and 6.7 in 1:2 ratios while the bridging ethylene signal comes at 9.7 ppm; Figure 13 shows the ^{1}H NMR spectrum of the molecule. The two broadest resonances are assigned as *meso* protons which are also confirmed by the ^{2}H NMR of the *meso*-deuterated μ-oxo dimer, **3**. The shifting of the methylene proton peaks by less than 0.5 ppm over the temperature range from 25 to −45 °C are also indicative of strong antiferromagnetic coupling between two iron(III) centers.

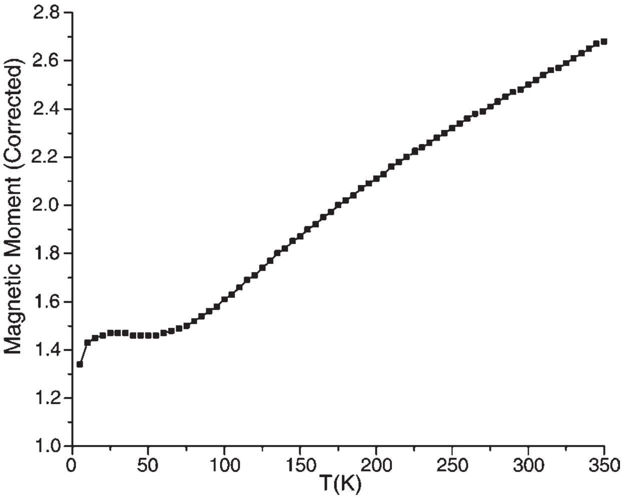

Figure 12. Magnetic moment of crystalline sample of **3** as a function of temperature.

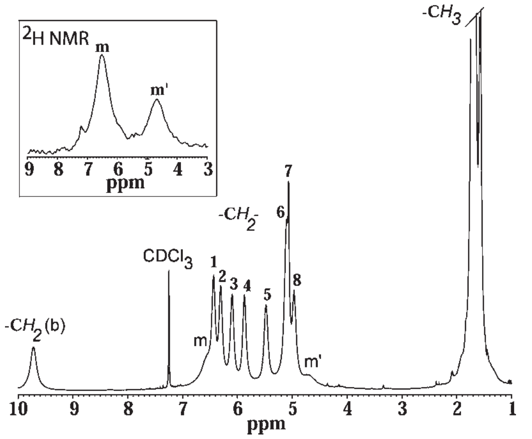

Figure 13. ^{1}H NMR spectrum of **3** in $CDCl_3$ at 295 K. Inset: ^{2}H NMR spectrum of *meso*-deuterated **3** in $CHCl_3$ at 290 K.

Because of highly strained geometry around oxygen, **3** shows some unusual reactivity which is not observed with the unbridged Fe(III)-μ-oxo dimer. The complex **3** is very inert to P(OR)$_3$ (R: Me, Et); however, photo irradiation ($\lambda_{exc} > 365$ nm, O−Fe LMCT transition) in the presence of excess phosphite in benzene solution under anaerobic conditions immediately changes its absorption spectra.[7] Moreover, each photoreaction yields a stoichiometric amount of O=P(OR)$_3$, as determined by ^{31}P NMR, and a single porphyrin product that is found to be diiron(II) bisporphyrin complex with axial phosphite ligands.[7]

Cyclic Voltammetric Study. Cyclic voltammetric experiments were carried out at 25 °C for **2** under N_2 in CH_2Cl_2 with 0.1 M tetrabutylammonium hexafluorophosphate

---

(21) (a) Jentzen, W.; Ma, J.-G.; Shelnutt, J. A. *Biophys. J.* **1998**, *74*, 753. (b) Jentzen, W.; Song, X.-Z.; Shelnutt, J. A. *J. Phys. Chem. B* **1997**, *101*, 1684.

(22) (a) Cheng, B.; Hobbs, J. D.; Debrunner, P. G.; Erlebacher, J.; Shelnutt, J. A.; Scheidt, W. R. *Inorg. Chem.* **1995**, *34*, 102. (b) Lee, H. M.; Olmstead, M. M.; Gross, G. G.; Balch, A. L. *Cryst. Growth Des.* **2003**, *3*, 691. (c) Scheidt, W. R.; Cheng, B.; Safo, M. K.; Cukiernik, F.; Marchon, J.-C.; Debrunner, P. G. *J. Am. Chem. Soc.* **1992**, *114*, 4420.

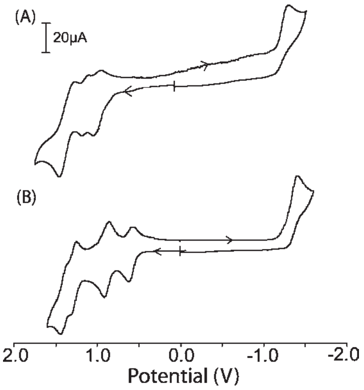

Figure 14. Cyclic voltammogram of (A) **2a** and (B) **3** in CH_2Cl_2 (scan rate 100 mV/s) with 0.1 M tetra(*n*-butyl)ammonium hexafluorophosphate as supporting electrolyte. The reference electrode was Ag/AgCl.

(TBAH) as the supporting electrolyte. Electrochemical data reveal that the complexes undergo two one electron and one two electron oxidations and one electron reductions, and a representative cyclic voltammogram is shown for **2a** in trace A of Figure 14. For example, cyclic voltammetric studies of **2a** in CH_2Cl_2 undergo two one-electron oxidations at 0.88 and 1.15 V because of the formation of mono and dication radicals, respectively, and one two electron oxidations at 1.44 V while the single one-electron reduction occurs at −1.34 V. Under identical condition, Fe^{III}(OEP)Cl shows two one electron oxidations at 0.92 and 1.35 V and one electron reduction at −0.97 V.[23] Thus, in **2a**, the oxidations become easier whereas reduction become harder than that of Fe^{III}-(OEP)Cl. This trend is also observed in other metalated bisporphyrins.[10c] As is apparent here, potentials are surprisingly insensitive to the nature of the anionic axial ligand, X (see Experimental Section).

The cyclic voltammogram of **3** also shows four reversible one electron oxidations at 0.57, 0.87, 1.27, and 1.39 V and one-electron reduction at −1.39 V; the spectrum is shown in trace B of Figure 14. Under identical conditions, $[Fe(OEP)]_2O$ shows similar oxidations at relatively higher potentials (at 0.65, 0.93, 1.30, 1.54 V) and reductions at slightly lower potential (−1.35 V). Also, oxidations are much easier in **3** than **2** while reduction occurs at similar potential. The presence of two porphyrin macrocycles within a short distance in the *syn* form makes the porphyrin core highly nonplanar and more electron rich, and that might be responsible for easier oxidations in **3** as observed before.[24]

Oxidation of 3. Coulometric oxidations are performed by applying a constant potential of 0.75 V for one electron oxidized species. Cyclic voltammetric waves for the oxidized product are identical with those for the parent iron(III) compound **3** demonstrating reversibility of the oxidations. The UV−visible spectrum of the monocationic species, **4**, also supports the assignment of a porphyrin π-cation radical; the intensity of the Soret band at 392 nm is lower and blue-shifted than that for the neutral μ-oxo complex, **3**, that comes at 402 nm. The blue shifting in the Soret band presumably reflects further closeness of the two porphyrin rings in the oxidized complex **4**.[22c] The visible bands are all broadened in the oxidized species as observed in some other systems.[25] Figure 15 compares the UV−vis spectra of both **3** and **4**. However, successful isolation of the oxidized complex **4** in pure state has not been realized by this method because of the presence of a large excess of supporting electrolytes.

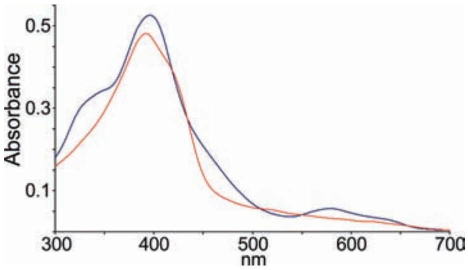

Figure 15. UV−vis spectra of μ-oxo dimer, **3** (blue line), one-electron oxidized product **4** (red line) at 298 K.

However, oxidation of iron(III) porphyrins by chemical oxidant of appropriate potential provides a ready means of generating the oxidized species which could not be isolated in pure form by coulometric oxidation. An iodine−silver perchlorate oxidizing agent has been utilized previously for generation of iron and zinc porphyrin π-cation radical species.[25] The one electron oxidized product **4** is also prepared by chemical oxidation using 1 equiv of iodine−silver perchlorate (see Experimental Section for details). Precipitated silver iodide is removed by centrifuge. The in situ one-electron oxidation yields products that are identical with those prepared by electrochemical oxidation. As expected, the singly oxidized complexes exhibit characteristic stretching frequencies for the ClO_4^- group at 619 and 1111 cm^{-1}. Their IR spectra also display the characteristic Fe−O−Fe stretching frequencies at 902 cm^{-1}, suggesting that the oxidized complex is in the μ-oxo form. It should be noted that neither iodine nor silver ion alone can oxidize **3** under identical conditions.

The oxidation of **3** in $CDCl_3$ using iodine−silver perchlorate has been monitored by ^1H NMR spectroscopy. Figure 16 shows the relevant spectra coming from the reaction between **3** and an acetonitrile solution of iodine−silver perchlorate. The data are presented so that the methylene and *meso* resonances which show large hyperfine shifts are visible. The methyl resonances, which occur in the diamagnetic region, have been cut off so that the others can be seen more readily. Trace A shows the spectrum of the oxo-bridged dimer, **3**, alone. The dimeric structure requires

---

[23] (a) Patra, R.; Chaudhary, A.; Ghosh, S. K.; Rath, S. P. *Inorg. Chem.* **2008**, *47*, 8324. (b) Patra, R.; Chaudhary, A.; Ghosh, S. K.; Rath, S. P. *Inorg. Chem.* **2010**, *49*, 2057.

[24] (a) Kadish, K. M.; Finikova, O. S.; Espinosa, E.; Gros, C. P.; Stefano, G. D.; Cheprakov, A. V.; Beletskaya, I. P.; Guilard, R. *J. Porphyrins Phthalocyanines*. **2004**, *8*, 1062. (b) Shelnutt, J. A. In *The Porphyrin Handbook*; Kadish, K. M., Smith, K. M., Guilard, R., Eds.; Academic Press: New York, 2000; Vol. *7*, p 167.(c) Kadish, K. M.; Guo, N.; Caemelbecke, E. V.; Paolesse, R.; Monti, D.; Tagliatesta, P. *J. Porphyrins Phthalocyanines*. **1998**, *2*, 439.

[25] (a) Kadish, K. M.; Autret, M.; Ou, Z.; Tagliatesta, P.; Boschi, T.; Fares, V. *Inorg. Chem.* **1997**, *36*, 204. (b) Balch, A. L.; Latos-Grażyński, L.; St. Claire, T. N. *Inorg. Chem.* **1995**, *34*, 1395. (c) Bottomley, L. A.; Gorce, J.-N. *Inorg. Chim. Acta* **1986**, *125*, 135. (d) Chang, D.; Cocolios, P.; Wu, Y. T.; Kadish, K. M. *Inorg. Chem.* **1984**, *23*, 1629. (e) Phillippi, M. A.; Goff, H. M. *J. Am. Chem. Soc.* **1982**, *104*, 6026. (f) Phillippi, M. A.; Shimomura, E. T.; Goff, H. M. *Inorg. Chem.* **1981**, *20*, 1322. (g) Phillippi, M. A.; Goff, H. M. *J. Am. Chem. Soc.* **1979**, *101*, 7641.

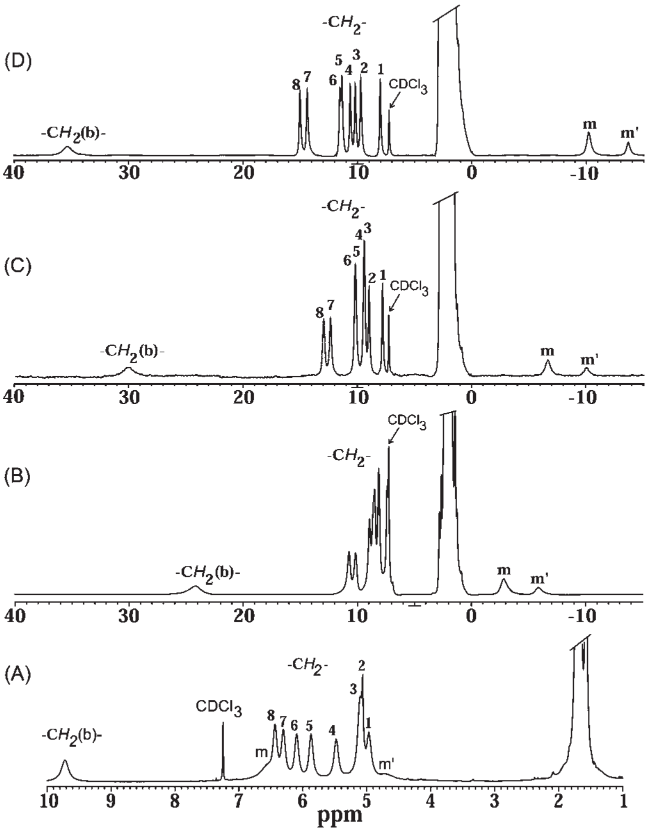

Figure 16. ^{1}H NMR spectra of the reaction of **3** in $CDCl_3$ with iodine−silver perchlorate in acetonitrile at 295 K. Trace A, **3**; trace B, after the addition of 0.25 mol equiv of iodine−silver perchlorate; trace C, after addition of 0.50 mol equiv of iodine−silver perchlorate. Trace D, after addition of 1.00 mol equiv of iodine−silver perchlorate forming **4**.

that there are two types of *meso* protons and four types of methylene groups. Within each of these methylene groups, the two protons are inequivalent. Consequently there are eight methylene resonances.

Trace B and C in Figure 16 shows ^{1}H NMR spectra after the addition of 0.25 and 0.50 mol equiv of iodine−silver perchlorate in acetonitrile, respectively. However, addition of a total 1.00 mol equiv of iodine−silver perchlorate produces the spectrum shown in trace D which corresponds to one electron oxidized product, **4**. The rapid intra- and intermolecular electron exchange yields average signals in B and C which match exactly by mixing appropriate concentrations of separately prepared singly oxidized dimer, **4**, with **3**. This indicates that electron transfer is rapid on the NMR time scale and no porphyrin structural modification has occurred during the oxidation. The eight diastereotopic methylene proton signals (at 295 K) spread over 8 to 16 ppm and two *meso* resonances occur at −10.2 and −13.7 ppm in 2:1 ratio, and also demonstrates the co-facial nature of the oxidized species **4** in solution. Small isotropic shifts in trace A reflect the weak paramagnetic character as a consequence of strong antiferromagnetic coupling through the oxo bridge. However, the singly oxidized species result in the upfield shift of the *meso* protons and the downfield shift of the ethylene protons and yield well-resolved ^{1}H NMR spectra (trace D) which differ from the parent Fe(III) spectra (trace A) most significantly in terms of larger isotropic shifts. The large isotropic shifts are overall suggestive of porphyrin π-cation radical character and also indicative of relatively weaker antiferromagnetic coupling between two iron centers as compared to **3**.[25d] As expected, bis Fe(III) μ-oxo porphyrin **3** exhibit low magnetic moments (2.5 μ_B per dimeric unit at room temperature) as a consequence of metal−metal antiferromagnetic coupling. However, for the one-electron oxidized product **4**, the effective magnetic moments per dimeric unit are 3.2 and 3.4 μ_B at 295 K in the solid and in dichlomethane, respectively. A radical center is normally expected to exhibit an ESR spectrum and induce extreme broadening of the ^{1}H NMR resonances. However, proximity of the paramagnetic iron atom should promote electronic relaxation to yield at best a very broad EPR spectrum and NMR signals which are not excessively broadened as found in **4**. Therefore, observation of well-defined NMR resonances in **4** does not necessarily preclude radical character in the species.[25d]

Conclusions

In the present work, we have utilized bis(octaethylporphyrin), **1**, bridged by highly flexible ethane which stabilizes both *syn* and *anti* forms. Bis Fe(III)porphyrins with axial ligand X (X: Cl, Br, I, ClO_4) are synthesized and characterized which authenticate the *anti*-form of the molecule. X-ray structure of *anti* bis perchloratoFe(III)porphyrin is reported here in which the Fe(III) center is in a high-spin state. In sharp contrast, all reported Fe(III) porphyrins with ClO_4^- axial ligands are either intermediate or admixed spin states. The very strong $Fe{-}OClO_3$ bond and relatively weaker Fe−N(p) bonds are responsible for the high-spin nature of the molecule. Upon treatment with 5% NaOH, **2** converts immediately to bis Fe(III)-μ-oxo porphyrin, **3**, in which Fe−O−Fe moiety is remarkably bent and two porphyrin rings in the molecule are so close that at least six carbon atoms from each of the porphyrin macrocycles are driven to be essentially less than the van der Waals contact distance. To a significant extent, the bending is promoted by the "outward" direction of the peripheral ethyl groups as well as the positioning of solvent molecules in between the rings. Upon manipulating the acidity/basicity of the solution, the facile conformational switching, between **2** and **3**, takes place in which the bisporphyrin platform "opens" and "closes" its binding pocket in a single molecular framework. The facile *syn-anti* conformational switching is indicative of small energy change that would lower the transition state energy for substrate activation as evidenced in its reactivity. Complex **3** catalyzes the photo induced oxygenation of phosphites under mild condition using aerial oxygen.

The complexes are redox active and undergo four electron oxidations and one electron reductions within the potential limits of dichloromethane. The presence of two porphyrin macrocycles within a short distance in the Fe(III)-μ-oxo porphyrin **3** makes the core highly nonplanar and more electron rich, and that might be responsible for easier oxidations in **3**. Oxidations of μ-oxo complex, **3**, are performed using both chemical and electrochemical methods. Addition of a total 1.00 mol equiv of iodine−silver perchlorate to the $CDCl_3$ solution of **3** produces the spectrum of singly oxidized product **4** which yields well resolved ^{1}H NMR spectra that results in the upfield shift of the *meso* protons and downfield shift of the ethylene proton. The large isotropic shifts observed here are overall suggestive of porphyrin π-cation

Table 4. Crystal Data and Data Collection Parameters of **2c**, **3a**, and **3b**

	2c	**3a**	**3b**
T, K	100(2)	100(2)	100(2)
formula	$C_{74}H_{92}Cl_2Fe_2N_8O_9$	$C_{76}H_{93}Fe_2N_9O$	$C_{77.5}H_{94}Fe_2N_8O$
formula weight	1420.16	1260.29	1265.31
crystal system	monoclinic	monoclinic	monoclinic
space group	*P*21	*P*21/*n*	*P*21/*n*
a, Å	11.485(4)	16.475(4)	16.4668(8)
b, Å	20.610(8)	15.317(3)	15.3828(7)
c, Å	14.784(5)	26.587(6)	26.7700(13)
α, deg	90	90	90
β, deg	99.118(7)	96.988(4)	97.3970(10)
γ, deg	90	90	90
V, $Å^3$	3455(2)	6659(3)	6724.6(6)
radiation (*λ*, Å)	Mo Kα (0.71073)	Mo Kα (0.71073)	Mo Kα (0.71073)
Z	2	4	4
d_{calcd}, g cm^{-3}	1.365	1.257	1.250
μ, mm^{-1}	0.561	0.488	0.483
F(000)	1500	2688	2700
no. of unique data	7700	12001	12496
no. of restraints	76	0	0
no. of params. refined	900	810	838
GOF on F^2	1.038	0.986	1.033
$R1^a$ [$I > 2\sigma(I)$]	0.0912	0.0664	0.0593
$R1^a$ (all data)	0.1311	0.0980	0.0983
$wR2^b$ (all data)	0.2421	0.1650	0.1576

$^a R1 = \sum||F_o| - |F_c||/\sum|F_o|$. $^b wR2 = [\sum w(F_o^2 - F_c^2)^2/\sum w(F_o^2)^2]^{1/2}$.

radical character of **4** in solution. However, the addition of 0.25 and 0.50 equiv of oxidizing agent gives an average ^1H NMR signal. This indicates that intra- and intermolecular electron transfer is rapid in the NMR time scale and no porphyrin structural modification has occurred.

Experimental Section

Materials. H_2OEP,[9a] 1,2-bis(*meso*-octaethylporphyrinyl)ethane, **1**,[9b] *anti*-1,2-bis[chloroiron(III) 5-(2,3,7,8,12,13,17,18-octaethylporphyrinyl)]ethane, **2a**,[8b] and *syn*-1,2-bis[*μ*-oxo iron(III) 5-(2,3,7,8,12,13,17,18-octaethylporphyrinyl)]ethane, **3**,[7] are prepared by modifying the literature methods. Reagents and solvents are purchased from commercial sources and purified by standard procedures.

***Anti*-1,2-bis[bromoiron(III) 5-(2,3,7,8,12,13,17,18-octaethylporphyrinyl)]ethane, 2b.** A 100 mg portion of **1** (0.091 mmol) was dissolved in a degassed solvent mixture of $CHCl_3$ (25 mL) and CH_3CN (50 mL) under dinitrogen atmosphere, and $FeBr_2$ (300 mg, 1.4 mmol) was added to it. The reaction mixture was then stirred under nitrogen atmosphere at 55 °C for 40 min. After cooling to room temperature, the mixture was washed with 5% aqueous HBr. The organic layer was then separated and dried over anhydrous Na_2SO_4 and evaporated to complete dryness. The solid, thus obtained, was dissolved in a minimum volume of dry CH_2Cl_2 and then carefully layered with *n*-hexane. On standing for 5−6 days, a dark brown crystalline solid was formed which was collected by filtration and dried in vacuum. Yield: 90 mg (77%). Anal. Calcd (found): C, 65.27 (65.32); H, 6.67 (6.72); N, 8.23 (8.18). UV−vis (dichloromethane) [λ_{max}, nm (ε, M^{-1} cm^{-1})]: 398 (1.5×10^5), 516 (2.4×10^4), 652 (1.3×10^4). EPR data: in solid (110 K), $g_\perp = 5.97$ and $g_\parallel = 1.99$; in dichloromethane (110 K), $g_\perp = 5.97$ and $g_\parallel = 1.99$. ^1H NMR ($CDCl_3$, 295 K): *meso-H*: −54.0, −72.2; $-CH_3$: 7.6, 7.9, 8.2; $-CH_2$: 36.7, 38.6, 39.8, 41.3, 44.6, 46.6, 53.0; $-CH_2$(b):77.9 ppm. $E_{1/2}$(ox), V (ΔEp, mV): 0.85(90), 0.97(75), 1.43(110); $E_{1/2}$(red), V: −1.39. μ_{eff} (295 K, crystalline solid), 5.86 μ_B per iron.

***Anti*-1,2-bis[chloroiron(III) 5-(2,3,7,8,12,13,17,18-octaethylporphyrinyl)]ethane, 2a.** EPR data: in solid (110 K), $g_\perp = 5.98$ and $g_\parallel = 2.00$; in dichloromethane (110 K), $g_\perp = 5.98$ and $g_\parallel = 2.00$. ^1H NMR ($CDCl_3$, 295 K): *meso-H*: −55.0, −74.7; $-CH_3$: 5.0, 6.9; CH_2: 35.3, 37.2, 39.7, 42.2, 44.1, 44.5, 48.1; CH_2(b):73.5 ppm. $E_{1/2}$(ox), V (ΔEp, mV): 0.88(100), 1.15(85), 1.44(120); $E_{1/2}$(red), V: −1.34. μ_{eff} (295 K, crystalline solid), 5.76 μ_B per iron.

Anti*-1,2-bis[perchloratoiron(III) 5-(2,3,7,8,12,13,17,18-octaethylporphyrinyl)]ethane, 2c.** A 100 mg portion of **2a** (0.079 mmol) was dissolved in 50 mL of benzene, and 33 mg (0.158 mmol) of $AgClO_4$ in 2 mL of benzene was added to it and stirred at room temperature for 1 h. The resulting solution was then evaporated to complete dryness. The solid was then dissolved in dichloromethane and filtered off the insoluble AgCl. The filtrate thus obtained was then evaporated to dryness. The resulting solid was dissolved in minimum volume of dry CH_2Cl_2 and then carefully layered with *n*-hexane. On standing for 5−6 days, dark brown crystalline solid was formed which was collected by filtration and dried in vacuum. Yield: 80 mg (72%). ***Caution! *Perchlorate salts are potentially explosive when heated or shocked. Handle them in milligram quantities with care.* Anal. Calcd (found): C, 63.41 (63.45); H, 6.48 (6.53); N, 8.00 (8.08). UV−vis (dichloromethane) [λ_{max}, nm (ε, M^{-1} cm^{-1})]: 390 (1.4×10^5), 410 (1.3×10^5), 515 (1.8×10^4), 647 (9.5×10^3). EPR data: in solid (110 K), $g_\perp = 5.95$ and $g_\parallel = 2.00$; in dichloromethane (110 K), $g_\perp = 5.95$ and $g_\parallel = 2.00$. ^1H NMR ($CDCl_3$, 295 K): *meso-H*: −35.2, −52.4; $-CH_3$: 6.2, 6.7; $-CH_2$: 34.0, 35.2, 36.9, 40.5, 44.3, 48.9, 49.3, 58.9; $-CH_2$(b): 64.5 ppm. μ_{eff} (295 K, crystalline solid), 5.83 μ_B per iron.

***Anti*-1,2-bis[iodoiron(III) 5-(2,3,7,8,12,13,17,18-octaethylporphyrinyl)]ethane, 2d.** A 100 mg portion (0.071 mmol) of **2c** was dissolved in 50 mL of dichloromethane, and 0.2 M aqueous KI solution was added to it. The mixture was then stirred at room temperature for 3 h. The organic layer separated out and dried over anhydrous Na_2SO_4. After filtration, the solution was evaporated to complete dryness and redissolved again in minimum volume of dry CH_2Cl_2 which was then carefully layered by *n*-hexane. On standing for 5−6 days, dark brown crystalline solids were obtained which were washed well with the mother liquor and dried in vacuum. Yield: 85 mg (82%). Anal. Calcd (found): C, 60.97 (61.07); H, 6.23 (6.30); N, 7.69 (7.72). UV−vis (dichloromethane) [λ_{max}, nm (ε, M^{-1} cm^{-1})]: 397 (1.4×10^5), 522 (2.1×10^4), 651 (9.5×10^3). EPR data: in solid (110 K), $g_\perp = 5.96$ and $g_\parallel = 1.99$; in dichloromethane (110 K), $g_\perp = 5.96$ and $g_\parallel = 1.99$. ^1H NMR ($CDCl_3$, 295 K): *meso-H*: −44.4, −59.3;

$-CH_3$: 6.6, 6.3; $-CH_2$: 37.1, 38.4, 41.5, 43.4, 44.7, 47.7, 49.3, 60.7; $-CH_2$(b): 77.1 ppm. $E_{1/2}$(ox), V (ΔEp, mV): 0.89(100), 1.03(90), 1.34(95); $E_{1/2}$(red), V: -1.43. μ_{eff} (295 K, crystalline solid), 5.80 μ_B per iron.

4. A 2.5 mg (0.01 mmol) sample of iodine in 0.5 mL of CH_2Cl_2 and 4.1 mg (0.02 mmol) of $AgClO_4$ in 0.1 mL of acetonitrile were added to 20 mg (0.016 mmol) of **3** in 2 mL of CH_2Cl_2. The mixture was stirred at room temperature for 15 min. After filtration of AgI the product was precipitated by adding *n*-hexanes. Yield: 13 mg (62%). ***Caution!*** *Perchlorate salts are potentially explosive when heated or shocked. Handle them in milligram quantities with care*. Anal. Calcd (found): C, 67.40 (67.44); H, 6.88 (6.93); N, 8.50 (8.46). UV−vis (dichloromethane) [$\lambda_{\max}$, nm (ε, M^{-1} cm^{-1})]: 392 (1.5×10^5), 518 (1.7×10^4); 621 (1.2×10^4). IR(KBr): νClO_4^-, cm^{-1}: 619, 1111. EPR data (dichloromethane, 110 K): $g = 1.99$. ^1H NMR ($CDCl_3$, 295 K): *meso-H*: -10.2, -13.7; $-CH_3$: 2.2, 2.4, 2.7, 2.9; $-CH_2$: 8.0, 9.7, 10.2, 10.6, 11.4, 11.6, 14.4, 15.0; $-CH_2$(b): 35.4 ppm.

Instrumentation. UV−vis spectra were recorded on a PerkinElmer UV/vis spectrometer. Elemental (C, H, and N) analyses were performed on CE-440 elemental analyzer. EPR spectra were obtained on a Bruker EMX EPR spectrometer. Cyclic voltammetric studies were performed on a BAS Epsilon electrochemical workstation in dichloromethane with 0.1 M tetrabutylammonium Hexafluorophoshate (TBAH) as supporting electrolyte. The reference electrode was Ag/AgCl, and the auxiliary electrode was a Pt wire. The concentration of the compounds was in the order of 10^{-3} M. The ferrocene/ferrocenium couple occurs at $E_{1/2} = +0.45$ (65) V versus Ag/AgCl under the same experimental conditions. Magnetic susceptibility data were collected using a Quantum Design MPMS SQUID magnetometer over the temperature range 5 to 300 K for **2b** and **3**. Data were collected in applied fields of 0.1 and 1 T for **2b** and **3**, respectively, and corrected for diamagnetism using Pascal's constants. ^1H NMR spectra were recorded on a JEOL 500 MHz instrument. The spectra for paramagnetic molecules were recorded over a 100 kHz bandwidth with 64K data points and a 5 μs 90° pulse. For a typical spectrum between 2000 and 3000 transients were accumulated with a 50 μs delay time. The residual ^1H resonances of the solvents were used as a secondary reference.

X-ray Structure Solution and Refinement. Crystals were coated with light hydrocarbon oil and mounted in the 100 K dinitrogen stream of Bruker SMART APEX CCD diffractometer equipped with CRYO Industries low-temperature apparatus, and intensity data were collected using graphite-monochromated Mo Kα radiation ($\lambda = 0.71073$ Å). The data integration and reduction were processed with SAINT software.[26] An absorption correction was applied.[27] Structures were solved by the direct method using SHELXS-97 and were refined on F^2 by the full-matrix least-squares technique using the SHELXL-97[28] program package. Non-hydrogen atoms were refined anisotropically. In the refinement, hydrogens were treated as riding atoms using SHELXL default parameters. For **2c**, the ClO_4 axial ligands are disordered and are distributed over two fractional occupancies (0.67(1) and 0.33(1) for Cl1 and 0.71(1) and 0.29(1) for Cl2). In all the cases, the occupancies were determined by refinement. Crystal data and data collection parameters for **2c**, **3a**, and **3b** are given in Table 4.

Acknowledgment. We are thankful to the Department of Science and Technology, Government of India for financial support. S.K.G. and R.P. thank CSIR, India, for their fellowships.

Supporting Information Available: X-ray crystallographic details in CIF format, and Table S1 containing the Normal Coordinate Structural Decomposition (NSD) of the complexes. This material is available free of charge via the Internet at http://pubs.acs.org.

---

[26] *SAINT+*, version 6.02; Bruker AXS: Madison, WI, 1999.

[27] Sheldrick, G. M. *SADABS 2.0*; University of Göttingen: Göttingen, Germany, 2000.

[28] Sheldrick, G. M. *SHELXL-97: Program for Crystal Structure Refinement*; University of Göttingen: Göttingen, Germany, 1997.